A Vessel-Agnostic Networked Sensor Suite for Autonomy on Inland Waterways*

Yan-Yun Zhang[a,b,*,1], Zhongbi Luo[a,1], Jef Billet[a], Senne Van Baelen[a], Jan Swevers[a,b], Herman Bruyninckx[a,b,c] and Peter Slaets[a]

[a]Department of Mechanical Engineering, KU Leuven, Leuven, 3001, Belgium
[b]Flanders Make@KU Leuven, Leuven, 3001, Belgium
[c]Department of Mechanical Engineering, TU Eindhoven, Eindhoven, 5612 AZ, The Netherlands

ARTICLE INFO

Keywords:
Integrated Sensor Suite
Autonomous Surface Vessels
Inland Waterway Transportation
Localization
Perception
Situation Awareness

ABSTRACT

This paper presents a modular, vessel-agnostic sensor suite called *Sensor Box*. It provides localization, perception and navigation-enabling capabilities that are fundamental to the automation of inland waterway transport. *Sensor Box* is designed to support research on the automation of operational inland surface vessels, providing the possibility to equip these vessels with the required sensors without the need for substantial retrofitting efforts. *Sensor Box* is organized into a three-layered hardware architecture with (i) onboard computing and power, (ii) positioning sensors and connectivity components, and (iii) perception sensors. We perform an intrinsic characterization and extrinsic calibration for all sensors, registering all measurements to a common spatial reference frame. All components are interconnected via an Ethernet network and exposed via a single network interface to a host vessel, with options for legacy gateways. Time-synchronized standardized sensor streams are exchanged through a publish-subscribe messaging framework using predefined message schemas and topic namespaces. Finally, we demonstrate *Sensor Box* in data-collection experiments on an inland test vessel and release the resulting multimodal dataset on the open Zenodo repository at https://doi.org/10.5281/zenodo.18829644.

Nomenclature

Sensors

AIS	Automatic Identification System
GNSS	Global Navigation Satellite System
GPS	Global Positioning System
IMU	Inertial Measurement Unit
INS	Inertial Navigation System
LiDAR	Light Detection And Ranging
RADAR	Radio Detection And Ranging

Data Formats and Protocols

BayerRG8	Bayer Red-Green filtered 8-bit unpacked pixel format
CAN	Controller Area Network, a standard protocol for communication between microcontrollers and devices over a shared bus
DIFOP	LiDAR Information Output Data Protocol, a proprietary protocol of RoboSense LiDARs
GGA	Global Positioning System Fix Data, a sentence type in the NMEA protocol containing time, position, and fix-related data
GigE Vision	Gigabit Ethernet Vision, a standard for high-speed video transmission
IP	Internet Protocol, a standard protocol for addressing and routing packets across networks
MSOP	Main Data Stream Output Data Protocol, a proprietary protocol of RoboSense LiDARs
NMEA	National Marine Electronics Association standard protocol for communication between marine electronic devices
NTRIP	Networked Transport of RTCM via Internet Protocol, a standard for streaming GNSS correction data over IP networks
RMC	Recommended Minimum Specific GNSS Data, a sentence type in the NMEA protocol
RTCM	Radio Technical Commission for Maritime Services standard format for transmitting GNSS correction data

*The development of the presented Sensor Box was supported by funding from the European Union's Horizon 2020 research and innovation programme under Societal Challenges - Smart, Green and Integrated Transport, grant agreement No. 861377 (IW-NET).

*Corresponding author.
yanyun.zhang@kuleuven.be (Y.Y. Zhang); zhongbi.luo@kuleuven.be (Z. Luo); jef.billet@kuleuven.be (J. Billet); senne.vanbaelen@kuleuven.be (S. Van Baelen); jan.swevers@kuleuven.be (J. Swevers); herman.bruyninckx@kuleuven.be (H. Bruyninckx); peter.slaets@kuleuven.be (P. Slaets)
ORCID(s): 0000-0002-6078-9213 (Y.Y. Zhang); 0009-0002-7899-735X (Z. Luo); 0000-0002-8003-1303 (J. Billet); 0000-0003-4624-3107 (S.V. Baelen); 0000-0003-2034-5519 (J. Swevers); 0000-0003-3776-1025 (H. Bruyninckx); 0000-0002-8560-2638 (P. Slaets)

[1]Funded by the European Union's Horizon 2020 research and innovation programme under Excellent Science - Marie Skłodowska-Curie Actions, grant agreement No. 955768 (AUTOBarge).

SBF	Septentrio Binary Format, a proprietary format of Septentrio GNSS receivers
TCP	Transmission Control Protocol, a standard protocol for data transmission over IP networks
UDP	User Datagram Protocol, a standard protocol for connectionless data transmission over IP networks

1. Introduction

Inland Waterway Transport (IWT) is a transport mode with substantially lower external costs from emissions, noise, and accidents compared to road-based transport Némethy et al. (2022). Consequently, facilitating a modal shift toward IWT is pivotal for advancing the green transition. In Europe, the navigable inland waterway network is extensive, spanning over 50,338 km Eurostat (2026). IWT has made significant progress in supporting Europe's economic growth and environmental sustainability Esposito (2024). However, the competitiveness of IWT is constrained by (i) slow diffusion of technological innovation, (ii) an ageing workforce and growing shortage of qualified skippers, and (iii) personnel costs that form a major component of operating costs, particularly for smaller vessels Gbako et al. (2025). These factors have sparked growing interest in advancing the autonomy level of Inland Surface Vessel (ISV).

Realizing autonomy in the inland shipping sector, however, presents significant challenges. A big challenge lies in the environmental complexity. Inland vessels operate in constrained and dynamic environments characterized by narrow fairways, dense and heterogeneous traffic, low-clearance bridges, and frequent interactions with infrastructure such as locks and quays. These conditions demand robust perception and accurate localization to ensure reliable situational awareness. Addressing such requirements necessitates the integration of advanced sensing hardware and corresponding algorithms capable of transforming raw sensor data into a structured, machine-interpretable representation of the navigational environment.

Another fundamental challenge lies in the absence of a systematic representation of inland vessel motion dynamics. The knowledge required to precisely maneuver a vessel in confined spaces, to interact safely with infrastructure, and to navigate in dense traffic remains largely experience-based, is confined to individual captains operating specific vessels on specific routes. Developing a transferable and machine-interpretable understanding of inland vessel behavior therefore requires mathematical models and data-driven approaches that can describe vessel motion in control-oriented input-output formulations.

Both challenges, situational awareness and vessel motion control, critically depend on the continuous availability of reliable onboard measurements. Autonomous operation requires real-time acquisition, processing, communication, fusion and interpretation of multimodal sensor data to maintain situational awareness and enable timely control decisions under dynamically changing conditions. Consequently, vessels must be equipped with comprehensive onboard instrumentation that integrates sensing, synchronization, data management, computation, and communication functionalities. To address this system-level hardware integration problem, two interrelated approaches exist.

The first focuses on **newbuild** autonomous inland vessels that are designed from the ground up to support rich sensing. Examples include *Roboat III* Wang et al. (2023), *milliAmpere* Brekke et al. (2022), *Solgenia* Homburger et al. (2025) and many others Peeters et al. (2020); Eide et al. (2025). These platforms are typically over-actuated and fully electric, equipped with built-in exteroceptive sensors that enable a multitude of facets of ISV autonomy, such as (simultaneous) localization and mapping Wang et al. (2020), docking Li et al. (2020); Homburger et al. (2024), and station-keeping Alfheim et al. (2018) methodologies.

In contrast stands Europe's operational inland fleet. It is old and heterogeneous, with the average age of an inland ship exceeding 40 years. Furthermore, newbuild activity is limited, slowing fleet renewal. This motivates the need for the complementary solution: **retrofitting** existing vessels with sensors and computing to unlock environmental and proprioceptive sensing without waiting for full remanufacturing cycles. Despite being more time and cost-effective compared to the newbuild approach, retrofitting the legacy vessels for autonomy remains challenging. Current integration practices are often tailored to a specific vessel, with a set sensor layout and a proprietary integration. As a consequence, technological innovations are difficult to reproduce or transfer between vessels, and significant engineering effort is repeatedly invested in non-reusable sensor infrastructure.

Together, these issues create a system-level hardware integration challenge in equipping heterogeneous legacy

vessels with reproducible, transferrable, and minimally invasive sensing infrastructure. As such, there is a clear need to consolidate sensors into a vessel-agnostic, self-contained suite that shortens calibration, cabling, and shipyard work, enabling sensoring hardware swaps without modifying the hull. Examples of this have been reported for the *milliAmpere* roof set-up Brekke et al. (2022) and the *Roboat III* sensor stack Wang et al. (2023). For the legacy inland fleet, adopting this *mount-once, move-often* approach cuts per-hull integration, avoids repeated calibration, and supports component-level upgrades while leaving the host vessel untouched. This enables small-scale installs across heterogeneous vessels Helgesen et al. (2022), providing localization, perception, communication, and systematic collection of motion datasets that are essential to research on these vessels.

In this work, we address the hardware integration challenge by introducing a robust and transferrable retrofitting solution: a vessel-agnostic sensor suite, hereafter referred to as *Sensor Box*, together with its reference integration on a test vessel named *Maverick* Zhang et al. (2023). *Sensor Box* is conceived as a portable sensing, computing, and communication package that can be installed on various platforms with minimal mechanical and electrical modifications, providing a common basis for research on surface vessel autonomy in inland waterways. While developed specifically for inland navigation, its modular, standalone design and platform-agnostic integration are not limited to the maritime domain. The proposed architecture is equally applicable to other autonomous vehicle platforms where retrofitting, reproducibility, and standardized data acquisition are required.

Sensor Box has been used successfully in recent research towards inland autonomy, including data-driven ship maneuvering modeling based on navigation data (Zhang et al. (2024)), extended object tracking via AIS and LiDAR fusion (Baerveldt et al. (2024)) and inland electronic navigational chart updating based on shoreline detection using LiDAR scans (Luo et al. (2024)). These studies demonstrate the versatility of the hardware platform across modeling, perception, and navigation domains.

In this work, we also introduce and describe the *Leuven Vaart Dataset*, recorded with *Sensor Box* that can help benchmarking inland navigation research. The dataset captures semi-structured operational environments characteristic of European canals, including transitions between natural vegetated banks and structural revetments, as well as vessel interactions with dynamic infrastructure such as a movable bascule bridge. These scenarios provide practical test cases for evaluating perception, mapping, and localization pipelines under diverse real-world conditions.

A distinctive feature of our dataset is its inclusion of partial LiDAR returns from the inland water surface. Inland waterways are commonly regarded as Z-axis degenerate environments for LiDAR-based localization, where LiDAR signals are largely absorbed, resulting in weakened vertical constraints and reduced structural observability near the waterline Chen et al. (2025). Allis et al. (2011) have shown that water surface detection remains feasible under specific turbidity and incidence angle conditions. Our dataset preserves these measurements. These surface returns provide valuable geometric cues that can support waterline boundary estimation, enhance scene reconstruction, and facilitate analysis of water-sensor interaction mechanisms in real-world settings.

The main contributions of this work are summarized as follows:

(i) **A transferable, vessel-agnostic *Sensor Box*.** We present the electromechanical design of a self-contained portable sensor suite together with a flexible communication architecture that provides the sensing, computing, and communication capabilities needed for autonomy.

(ii) **A step towards a shared ecosystem for autonomous surface vessel research.** By standardizing data formats and the communication interface, we lower the barrier for field experimentation and facilitate reproducible research within the community. The collected multi-sensor datasets are openly published to support collaborative development and benchmarking.

The remainder of this paper is structured as follows. Section 2 presents the physical design and components of *Sensor Box*. Section 3 details the calibration procedures and time synchronization scheme used to align all sensor data in space and time. Section 4 describes the modular and scalable communication and data distribution architecture of *Sensor Box*. Section 5 details the deployment of *Sensor Box* on *Maverick*, and describes the structure of the openly released dataset. Finally, Section 6 concludes the paper.

Table 1
Component overview of *Sensor Box*, categorized by structural layer.

Layer	Description	Selected Models	Cost [€]
Computation Bay	Battery	Mastervolt MLI-E 12/1200	1,995.00
	Battery Charging System	Mastervolt ChargeMaster 12/25–3	349.95
	Inverter	Mean Well TS-400-224B	157.00
	PLC	Siemens LOGO! 8	95.00
	Industrial Computer	OnLogic MK150B-53	1,350.36
	Switch-2	TP-Link TL-SG108PE	50.95
Navigation Deck	5G Antenna	Siretta Tango 44	43.14
	Router	DIGI IX10	441.65
	Switch-1	Netgear GS108	28.99
	GNSS/INS Receiver	Septentrio AsteRx-i3 D Pro+	4,900.00
	IMU	Analog Devices ADIS16505-2	-*
	GNSS Antenna (×2)	Tallysman TW7972	301.13
	Antenna Splitter (×2)	GPS Networking LDCBS1X2	300.00
	AIS Receiver	Raymarine AIS350	418.99
	AIS Antenna	Glomex RA106SLSSB18	129.95
	LiDAR Processing Unit	RoboSense Interface Box	73.76
	Battery Monitor Screen	Mastervolt EasyView 5	299.95
Perception Mast	LiDAR	RoboSense RS-Helios-5515	2,612.24
	Camera (×2)	Baumer VCXG.2-51C.I	1,165.00
	Camera accessories (×2)	Cabling, Adapters, etc.	1,279.57

* The IMU comes together with the GNSS/INS receiver.

2. Design and Components

Dimensionally, *Sensor Box* is a rectangular structure measuring 1.62 m × 0.20 m × 0.63 m (length × width × height), topped by a mast of 1.0 m in height. It is structured into three vertically stacked layers, each dedicated to a specific set of functional components: the *Computation Bay*, the *Navigation Deck*, and the *Perception Mast*. This physical separation improves maintainability and modularity, and allows the layers to be used independently when required.

An overview of the components and layout of *Sensor Box* is provided in Fig. 1. Panel (1a) gives a perspective view with structural frames rendered semi-transparent, highlighting the installed location and coordinates of key internal components. Panel (1b) presents a cutaway side view, in which the three layers are visually detached and highlighted using colored blocks. Table 1 lists all components, their model specifications and unit costs, grouped by structural layer. The total cost is approximately €20,000.00.

The specific composition and design rationale of each layer are detailed below:

(i) **Computation Bay**
The bottom layer (1.62 m × 0.20 m × 0.41 m) houses the primary power and processing components of *Sensor Box*. It includes a 1200 Wh Direct Current (DC) battery, managed by a dedicated charging system. Power conversion is handled by an inverter that supplies Alternating Current (AC) power to relevant devices. A Programmable Logic Controller (PLC) oversees power distribution and controls the switching of major electronic devices. An industrial computer, running a Linux Ubuntu-based operating system, performs data processing, logging, and communication tasks. A network switch (Switch-2) interconnects all devices in this bay and links them both to the other structural layers and to external systems when needed.

(ii) **Navigation Deck**
The middle layer (1.62 m × 0.20 m × 0.22 m) is dedicated to connectivity and positioning. All antennas are mounted on its top to ensure optimal signal reception. A cellular router provides 4G/5G connectivity for remote monitoring and data transmission. The core sensor of this layer is the GNSS/INS receiver, which provides high-accuracy positioning and attitude estimation. The chosen model, AsteRx-i3 D Pro+ by Septentrio, is a compact, lightweight GNSS receiver board that integrates a high-performance IMU (ADIS16505 by Analog Devices). It supports quad-constellation, multi-frequency, all-in-view Real Time Kinematics (RTK) positioning, providing full access

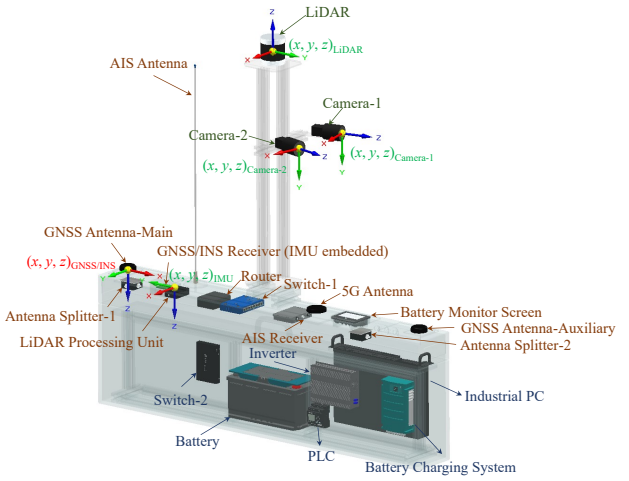

(a) Perspective view

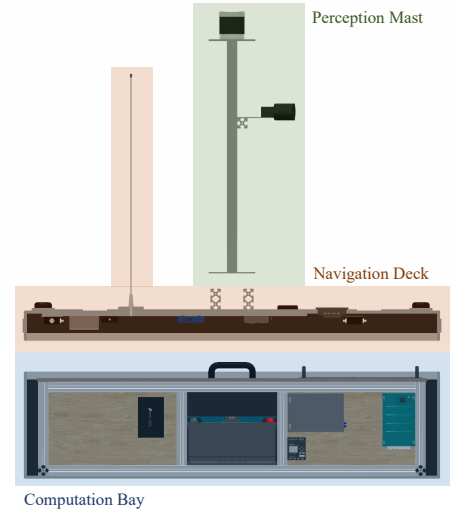

(b) Cutaway side view

Figure 1: Overview of *Sensor Box* with internal components and structural layout.

to raw measurements from GNSS and IMU separately, as well as a fused solution via a built-in extended Kalman filter. Dual GNSS antennas, installed with a 1.54 m baseline, ensure accurate heading estimation. Antenna splitters are used to allow expansion to additional GNSS devices if required. This layer also includes an AIS receiver for maritime traffic awareness, a RoboSense interface box for LiDAR data handling, and a battery monitor screen on the top panel for real-time monitoring of battery status.

(iii) **Perception Mast**

The topmost layer contains the primary perception sensors: the LiDAR and cameras. This elevated placement reduces occlusions from nearby structural elements and improves the detection of overhead targets such as bridges: the LiDAR is elevated by 1.0 m above the top surface of the enclosure, while the cameras are elevated by about 0.7 m. The selected LiDAR model, RS-Helios-5515 by RoboSense, is a 32-beam rotating sensor that provides a full 360° horizontal Field Of View (FOV) and a non-uniform 70° vertical FOV, ranging from +15° above to −55° below the sensor horizon. This asymmetrical vertical FOV, with a dominant portion directed downward, enhances coverage of the area surrounding the deployed platform and mitigates blind zones in the near field. Complementing the LiDAR, two industrial GigE Vision cameras (VCXG.2-51C.I by Baumer) operate at a resolution of 1280×720 pixels, providing visual information.

Each layer of *Sensor Box* can be used independently or in combination with the others, depending on mission requirements. For instance, the *Computation Bay* may be used as a standalone processing and autonomy unit for vessels already equipped with sensors; the *Navigation Deck* can serve as a separate portable positioning module when paired with a laptop; and the *Perception Mast* can be deployed as a dedicated perception package. This modularity enables flexible deployment and easy adaptation to a wide range of platforms and operational scenarios. In this work, our main usage scenario is to deploy the complete *Sensor Box* on the test vessel *Maverick*, with integration details described in Section 5.

Sensor Box is designed for outdoor deployment in inland waterway environments, including exposure to spraying water in the form of rainfall and splashing water resulting from vessel motion and wake. As illustrated in Fig. 1, all sensitive electronic components are housed within a sealed enclosure to prevent the ingress of water. Antennas and the battery monitoring display are mounted on the enclosure surface to maintain signal quality and operational accessibility. Their mechanical and electrical interfaces are sealed using appropriate cable glands to preserve enclosure integrity and prevent moisture ingress. The LiDAR and cameras are directly exposed to the environment, but their certified ingress protection ratings (LiDAR: IP67 and IP6K9K; camera housing: IP65/67) ensure reliable operation under the expected

conditions. The overall design of *Sensor Box* is robust and suitable for the intended operational environment.

3. System Calibration and Synchronization

Multi-sensor fusion requires knowledge of individual sensor intrinsics and the system's spatial and temporal relationships. This section details the methodology used to establish *Sensor Box* as a coherent multi-sensor system. We describe the intrinsic characterization of sensor-specific properties, the extrinsic calibrations that transform distributed sensor data into a common coordinate frame, and the synchronization architecture that aligns these data streams in the time domain. A summary of the calibration results is available in the openly available dataset under the calibration folder.

3.1. Intrinsic Calibration

Before establishing the spatial relationships between sensors, it is needed to characterize the intrinsic parameters of each sensor. This phase addresses the stochastic modeling of the IMU and the geometric correction of the cameras. For the LiDAR, no additional intrinsic calibration is performed, as it operates based on factory-calibrated parameters whose accuracy is sufficient for the intended applications. Similarly, the GNSS antenna phase center offsets and variations are corrected by the manufacturer-specified proprietary models. The AIS receiver, which functions as a digital communication system rather than a geometric sensor, does not require intrinsic calibration.

3.1.1. Inertial Stochastic Modeling

To accurately characterize the IMU's stochastic properties, its intrinsic noise parameters were derived via Allan Variance Allan (1966) analysis. We processed over three hours of stationary data using the *Allan Variance ROS* package, developed by Buchanan (2021). The continuous-time noise densities for the gyroscopes and accelerometers were quantified as 4.1×10^{-3} °/s/$\sqrt{\text{Hz}}$ and 3.2×10^{-4} m/s^2/$\sqrt{\text{Hz}}$, respectively, while the corresponding bias random walk coefficients were determined as 3.0×10^{-4} °/s^2/$\sqrt{\text{Hz}}$ and 1.9×10^{-5} m/s^3/$\sqrt{\text{Hz}}$.

3.1.2. Camera Geometric Intrinsics

The intrinsic parameters (focal length, principal point, and lens distortion coefficients) were estimated using the *Camera Calibration Toolbox*, provided by MathWorks (2025), with a standard 12×9 checkerboard target. Initial parameter estimates were derived for each camera individually. These intrinsics were subsequently refined via a unified optimization process alongside the stereo baseline. The global accuracy of the visual system is reported later in Section 3.2.3. The final refined parameters are fixed and utilized to correct lens distortion in the raw images.

3.2. Extrinsic Calibration

As each sensor acquires measurements in its local coordinate frame, extrinsic calibrations are required to determine the relative rigid-body transformations between the sensors. This also allows bringing all measurements into a single system reference frame. The AIS receiver is excluded from this process as it operates on broadcast messages independent of the ego-vessel's kinematic state.

3.2.1. Coordinate Systems and Mathematical Notation

The coordinate definitions for all sensors are illustrated in Fig. 1a. We define $(x, y, z)_{\text{GNSS/INS}}$ as the *body frame* ($\boldsymbol{B}$). Its origin coincides with the phase center of the main GNSS antenna, providing a stable georeferenced anchor. The frame orientation adheres to the standard maritime convention (Forward-Starboard-Down), aligned with the intended mounting orientation of *Sensor Box* on the host vessel.

Mathematically, the spatial relationship from a source frame $\boldsymbol{S}$ to a target frame $\boldsymbol{T}$ is expressed by the rigid-body transformation matrix $\boldsymbol{T}_{\text{T}\leftarrow\text{S}} \in \text{SE}(3)$:

$$\boldsymbol{T}_{\text{T}\leftarrow\text{S}} = \begin{bmatrix} \boldsymbol{R}_{\text{T}\leftarrow\text{S}} & \boldsymbol{t}_{\text{T}\leftarrow\text{S}} \\ \boldsymbol{0} & 1 \end{bmatrix} \tag{1}$$

where $\boldsymbol{R}_{\text{T}\leftarrow\text{S}} \in \text{SO}(3)$ denotes the rotation matrix and $\boldsymbol{t}_{\text{T}\leftarrow\text{S}} \in \mathbb{R}^3$ represents the translation vector.

To relate sensors not directly connected in the calibration chain, we use the compounding property of homogeneous transformations. For a sequence of frames $\boldsymbol{A}$, $\boldsymbol{B}$, and $\boldsymbol{C}$, the direct transformation $\boldsymbol{T}_{\text{A}\leftarrow\text{C}}$ is derived via matrix multiplication:

$$\boldsymbol{T}_{\text{A}\leftarrow\text{C}} = \boldsymbol{T}_{\text{A}\leftarrow\text{B}}\, \boldsymbol{T}_{\text{B}\leftarrow\text{C}} \tag{2}$$

This property allows the full extrinsic hierarchy (e.g., LiDAR → Camera → IMU → Body) to be resolved into a unified reference frame.

3.2.2. IMU–Body Calibration ($T_{B\leftarrow IMU}$)

The GNSS/INS receiver board is mounted parallel to *Sensor Box* enclosure's principal axes, simplifying the determination of the rotational alignment $\boldsymbol{R}_{B\leftarrow IMU}$. The translation vector $\boldsymbol{t}_{B\leftarrow IMU}$, representing the lever arm between the inertial measurement center and the antenna phase center, was initially measured manually using a laser rangefinder. These parameters were subsequently validated and refined using the *RxLeverArm* estimation tool, provided by the manufacturer Septentrio (2024).

3.2.3. Visual–Inertial Calibration ($T_{IMU\leftarrow Camera-i}$)

As there are two cameras in the visual system, we first determine the stereo baseline and then register the primary camera (Camera-1) to the inertial frame. The calibration is thus performed in two stages:

(i) **Stereo Baseline Estimation ($T_{Camera-1\leftarrow Camera-2}$):** The extrinsic relationship between the primary (Camera-1) and secondary (Camera-2) cameras was determined jointly with the intrinsic parameters of both cameras, as described in Section 3.1.2. This unified optimization achieved a global Mean Reprojection Error (MRE) of 0.68 pixels.

(ii) **Camera-1 to IMU Registration ($T_{IMU\leftarrow Camera-1}$):** The rigid-body transformation between the primary camera and the inertial frame was estimated using the *Kalibr* toolbox, developed by Furgale et al. (2013). We selected this toolbox because it accounts for intra-frame motion in continuous time and explicitly estimates temporal offsets between the sensors, thereby enabling highly accurate calibration. The calibration procedure involved sufficiently rich 6-Degree of Freedom (DoF) motion, including rotations about all axes and translations along all directions, to ensure full observability of the metric scale, gravity direction, and the sensor extrinsics. The optimization minimized feature reprojection residuals, resulting in a MRE of 1.25 pixels.

Consequently, the pose of the secondary camera relative to the IMU is computed via the chain rule: $\boldsymbol{T}_{IMU\leftarrow Camera-2} = \boldsymbol{T}_{IMU\leftarrow Camera-1} \cdot \boldsymbol{T}_{Camera-1\leftarrow Camera-2}$.

3.2.4. LiDAR–Visual Calibration ($T_{Camera-1\leftarrow LiDAR}$)

To estimate the rigid-body transformation between the LiDAR and the primary camera (Camera-1), we employed the *FAST-Calib* algorithm using a calibration target with circular cutouts, as described in Zheng and Zhang (2025). The cut-out holes provide both sharp physical depth discontinuities and continuous geometric edges, which are superior to intensity-based features for laser scanning. This design enables robust feature extraction of hole centers even with sparse LiDAR point clouds. The calibration pipeline first detects fiducial markers in the images to locate the 2D hole centers. Simultaneously, the algorithm extracts hole edges from the point cloud depth jumps to resolve the corresponding 3D hole centers. The extrinsic parameters were determined by minimizing the alignment error between these 2D-3D correspondence hole center pairs. The optimization yielded a root mean square point-to-point registration error of 1.75 cm. To illustrate the calibration success, Fig. 2 presents a validation example by projecting the LiDAR point cloud onto the image plane using the estimated $\boldsymbol{T}_{Camera-1\leftarrow LiDAR}$. The points are color-coded by their distance from the camera center, demonstrating consistent alignment with physical boundaries.

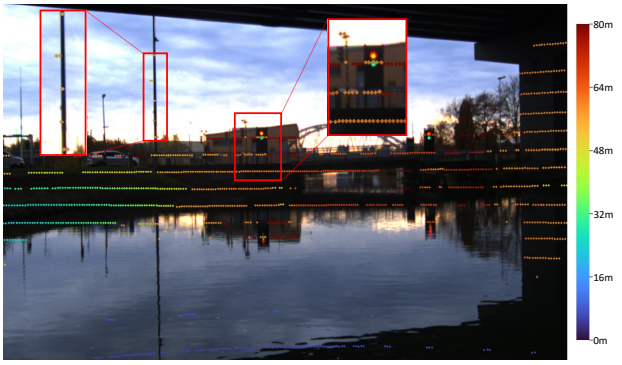

Figure 2: Validation of the LiDAR-visual extrinsic calibration.

3.3. Time Synchronization

Precise temporal alignment is critical to associate heterogeneous measurements with the same physical instant. *Sensor Box* employs a hierarchical synchronization scheme with the GNSS/INS receiver acting as the master clock, providing both a hardware Pulse Per Second (PPS) signal and GPS-referenced Coordinated Universal Time (UTC) timestamps. Fig. 3 summarizes the synchronization topology and data acquisition rates of the sensors, showing that all data streams are temporally referenced to the GNSS master clock.

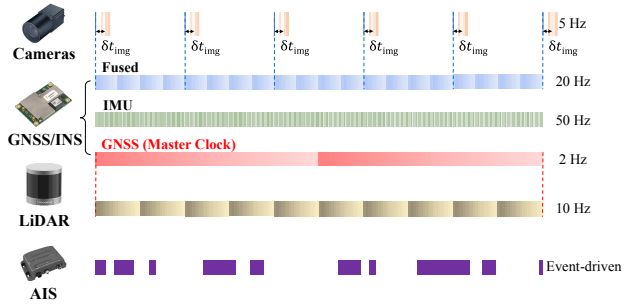

Figure 3: Overview of Sensor Synchronization and Data Acquisition Rates.

3.3.1. *Hardware-Level Synchronization (GNSS, IMU, LiDAR)*

The GNSS/INS receiver internally synchronizes its raw observables (up to 2 Hz), IMU measurements (up to 200 Hz), and the fused navigation solution (up to 100 Hz) to the GPS clock. The LiDAR unit is integrated into this domain via a direct hardware link. It utilizes the PPS signal to reset its internal microsecond counter at the top of each second and parses the NMEA RMC sentence (format defined in National Marine Electronics Association (2023)) to align with the correct UTC epoch. This mechanism ensures the LiDAR's internal clock tracks the master clock with sub-microsecond precision.

3.3.2. *Hybrid Triggering (Cameras)*

The camera system utilizes a primary-secondary hybrid triggering topology to ensure frame-level synchronization. Throughout this section, Δt denotes a time interval, i.e., the duration of an individual process, while δt denotes the time offset between two temporal references.

Trigger Generation and Propagation The system clock is synchronized to the GNSS time base using *Chrony*, developed by Curnow and Lichvar (2025), with a synchronization offset $\delta t_{\text{sync}} \approx 8\,\text{ms}$ between the system clock and the GNSS time base. The system parses NMEA GGA messages and generates software triggers for Camera-1 at 5 Hz. By pinning the process to a dedicated central processing unit core, the software triggering latency is bounded to $\Delta t_{\text{trig}} \approx 2\,\text{ms}$. Upon activation, Camera-1 acts as the primary node, propagating a hardware pulse to Camera-2 (the secondary node) via dedicated sync lines with a propagation latency denoted as Δt_{prop}.

Time Offset Decomposition The total system time offset, δt_{lag}, represents the time offset between the reference timestamp decoded from the NMEA GGA sentence (t_{gga}) and the completion timestamp of the image data available in the system memory (t_{end}). Since both timestamps are recorded for each frame, δt_{lag} is directly observable from the data. However, neither t_{gga} nor t_{end} corresponds to the physical instant of image acquisition, which lies at the middle of the exposure window. To estimate this instant, we decompose δt_{lag} into two distinct phases:

$$\delta t_{\text{lag}} = \underbrace{(\Delta t_{\text{trig}} + \Delta t_{\text{prop}} + \Delta t_{\text{shutter}} + \delta t_{\text{sync}})}_{\delta t_{\text{acq}}} + \underbrace{(\Delta t_{\text{readout}} + \Delta t_{\text{trans}})}_{\Delta t_{\text{post}}} \tag{3}$$

(i) **Acquisition Time Offset (δt_{acq}):** This component includes the offset before the completion of the exposure window comprising the trigger latency Δt_{trig}, the hardware propagation Δt_{prop} (applied to Camera-2), the exposure duration $\Delta t_{\text{shutter}}$, and the synchronization offset δt_{sync}.

(ii) **Post Capture Latency (Δt_{post}):** This component includes delays occurring after exposure, specifically the sensor readout latency $\Delta t_{\text{readout}}$ and the Ethernet transmission delay Δt_{trans}.

Experimentally, $\Delta t_{\text{post}} \approx 50\,\text{ms}$ is observed as the post-capture processing delay occurring after the exposure window, which does not alter the physical instant of acquisition. The middle of the exposure time $t_{\text{img}}^{(k)}$ for frame k, expressed in the GNSS time base, is obtained by:

$$t_{\text{img}}^{(k)} = t_{\text{end}}^{(k)} - \Delta t_{\text{post}} - \delta t_{\text{sync}} - \frac{\Delta t_{\text{shutter}}}{2} \tag{4}$$

Fig. 4 illustrates the resulting image time offsets $\delta t_{\text{img}}^{(k)} = t_{\text{img}}^{(k)} - t_{\text{gga}}^{(k)}$ for both cameras relative to the GNSS master clock. The observed jitter is mainly attributed to fluctuations in δt_{sync} and Δt_{trig}. Since Δt_{post} is approximated as a constant, fluctuations in sensor readout and Ethernet transmission also propagate into the estimated offsets. Primary-secondary triggering ensures tight synchronization ($\Delta t_{\text{prop}} < 1\,\text{ms}$), making stereo pairs temporally consistent. Although minor temporal uncertainty remains (on the order

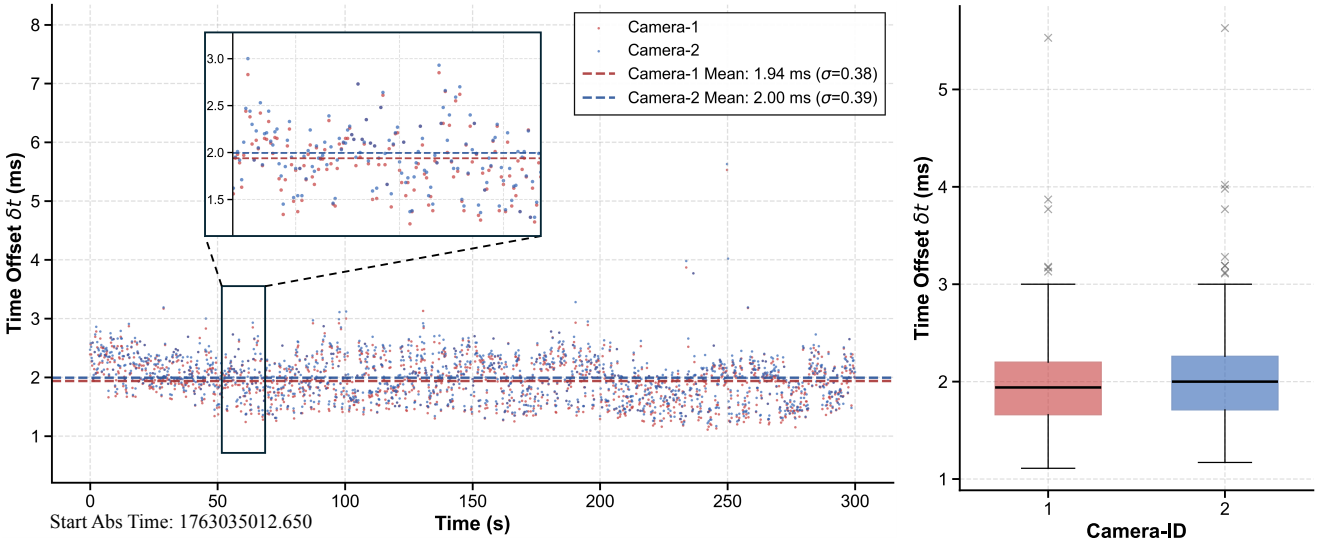

(a) Frame-wise time offsets δt_{img} relative to the GNSS master clock

(b) Distribution of time offsets

Figure 4: Overview of camera time synchronization performance.

of milliseconds), this accuracy is sufficient for the intended inland navigation tasks.

3.3.3. Event-Driven Synchronization (AIS)

The AIS communication protocol relies on GPS time for signal coordination. Consequently, incoming data packets are treated as aligned with the system's master clock, eliminating the need for additional temporal calibration. Nevertheless, standard AIS messages encode only a truncated 6-bit timestamp representing the second (0 … 59) of the current minute. To reconstruct the full global timestamp, this partial value is aligned with the most recent minute epoch provided by the master clock. The AIS receiver functions as an event-driven node, with a dynamic output rate determined by the frequency of packet arrival from surrounding vessels.

4. Communication and Data Distribution Architecture

To fulfill the requirement of a vessel-agnostic reference infrastructure, *Sensor Box* employs a communication architecture designed for modularity, scalability, and seamless interoperability with legacy marine systems. This section describes the dual-layer interface: (i) a physical *Ethernet-based backbone* that connects the sensor payload (Section 4.1), and (ii) a logical *publish–subscribe communication model* that standardizes data exchange (Section 4.2).

4.1. Hardware Architecture: The Ethernet Backbone

The hardware topology adopts an "Ethernet-first" design philosophy. Legacy inland vessels typically rely on fragmented standards, such as *NMEA 2000* National Marine Electronics Association (2022) for navigation and *SAE J1939* SAE International (2023) for machinery over CAN networks, while older equipment still uses *NMEA 0183* National Marine Electronics Association (2023) over serial connections. Increasingly, inland vessels adopt Ethernet in pursuit of higher bandwidth and lower latency, with gateways to the aforementioned interfaces using UDP multicast, as specified in *IEC 61162-450* International Electrotechnical Commission (2024) and *NMEA OneNet* National Marine Electronics Association (2024). Modern automation requirements align naturally with this trend. By standardizing on industrial Ethernet, *Sensor Box* minimizes integration overhead and ensures scalability for future applications, including real-time monitoring, remote control, predictive maintenance, and cloud-based connectivity.

Fig. 5 illustrates the physical interconnections of key electronic components within *Sensor Box*. The Industrial PC (IPC) acts as the central node, aggregating data from multiple sources via Ethernet through a switch. Specific design considerations include:

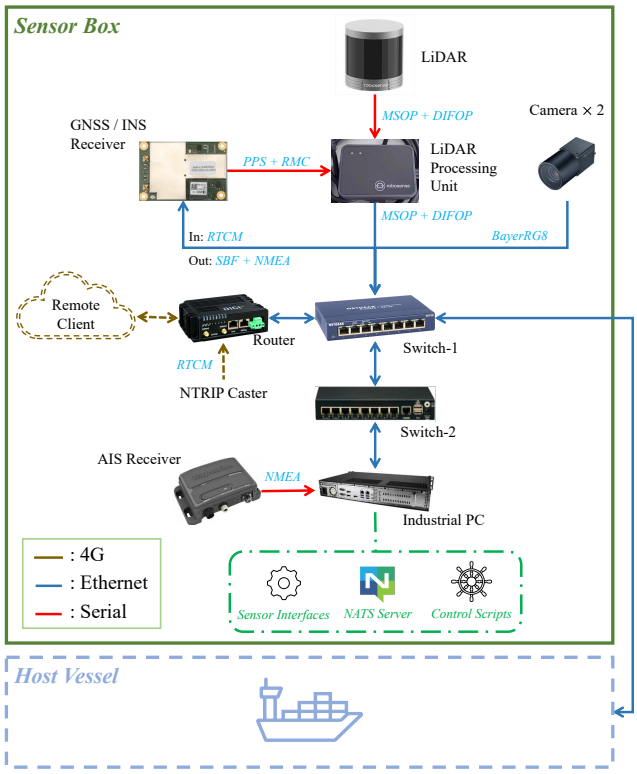

Figure 5: Hardware topology of *Sensor Box* with an Ethernet backbone.

(i) **High-bandwidth sensors:** Internal serial links connect the LiDAR to its processing unit and provide synchronization between the LiDAR and the GNSS/INS receiver, while bulk navigation and perception data are offloaded directly over the Ethernet to support high data throughput.

(ii) **Legacy interfaces:** The AIS receiver, operating on the legacy NMEA 0183 serial standard, is currently interfaced directly to the IPC, although the architecture supports future encapsulation via Ethernet gateways.

(iii) **Connectivity:** A cellular router provides a Wide Area Network (WAN) link to receive RTCM signals (essential for RTK correction in GNSS signals) and remote access.

Sensor Box connects to a host vessel's existing infrastructure following a "plug-and-play" concept: it remains a self-contained unit, requiring only a single Ethernet link to the vessel's gateway to access actuation and machinery status.

4.2. Software Architecture: The Publish–Subscribe Communication Model

To decouple hardware drivers and data streaming from autonomy applications, the software stack is structured around a publish–subscribe messaging framework that enables modular and distributed inter-process communication. This communication layer provides structured message transport, topic-based routing, and asynchronous data exchange between sensing, processing, and control modules. The primary functional requirements of this communication layer are:

(i) Low-latency message delivery suitable for real-time navigation and control.

(ii) Support for high-bandwidth sensor data streams.

(iii) Platform-agnostic communication across distributed computing nodes.

(iv) Scalability to accommodate additional sensors and processing modules.

The communication model is implemented using the NATS messaging system Synadia Communications Inc. (2025). However, the design remains implementation-agnostic, such that alternative publish–subscribe messaging systems can be integrated without modifying higher-level application modules. By isolating device-specific drivers behind this communication layer, downstream algorithms (e.g., state estimation, path planning, control, and data logging) remain independent of specific hardware interfaces and communication mechanisms.

4.2.1. Standardized Sensor Stream and Topic Model

On top of the communication model, a standardized *Sensor Stream* abstraction is defined for *Sensor Box*. This stream broadcasts time-synchronized perception and localization data in a set of structured message topics. As illustrated in Fig. 6 raw sensor data are parsed by dedicated interface nodes according to predefined message schemas and published under standardized topic namespaces. Downstream consumers subscribe only to relevant topics, enabling modular integration of autonomy applications, data loggers, or remote clients without dependence on device-specific protocols. Table 2 summarizes the defined topic namespaces, each corresponding to a specific sensor modality.

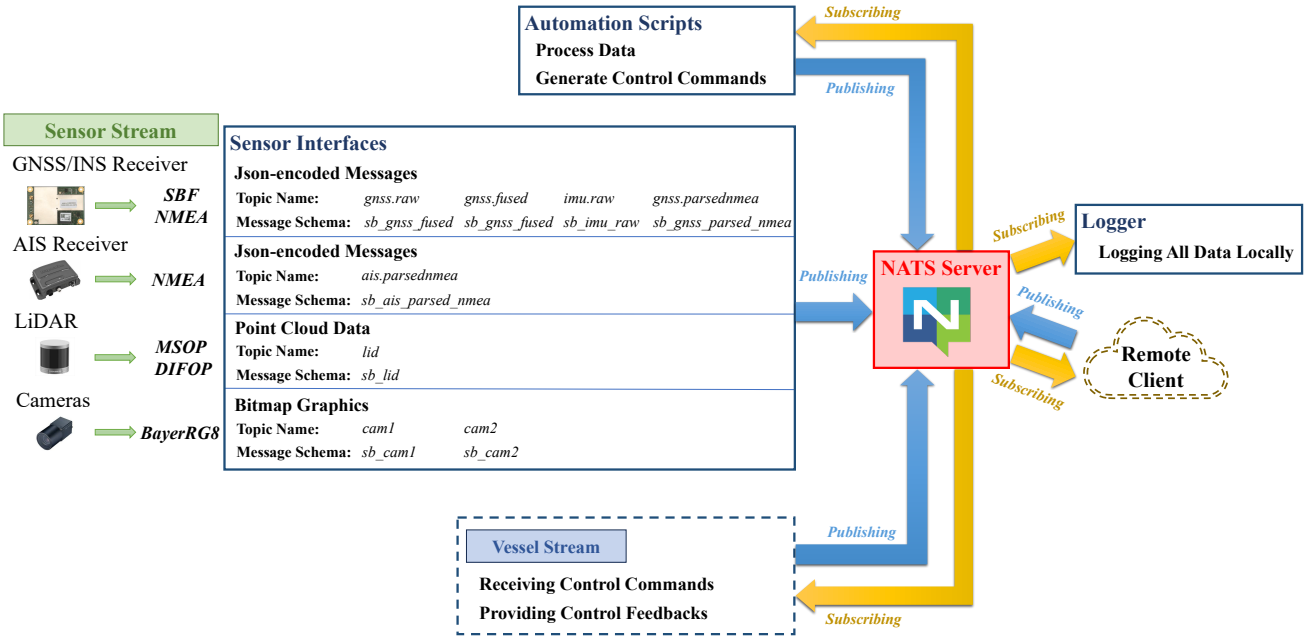

Figure 6: NATS-Implemented Software Architecture for *Sensor Box*.

Table 2
Standardized topic namespaces for *Sensor Box* data streams.

Topic namespace	Content description
`gnss.fused`	Fused GNSS-INS solution with improved accuracy and higher sampling rate.
`gnss.raw`	Raw GNSS solution with position, velocities, attitude, and accuracy/covariance terms.
`gnss.parsednmea`	Best available receiver solution parsed from NMEA sentence.
`imu.raw`	Raw IMU data on linear accelerations and angular rates.
`ais.parsednmea`	Surrounding vessel traffic information (identity, position, motion, integrity).
`lid`	3D point-cloud frames (XYZ with intensity/return fields).
`cam{1,2}`	Image frames from camera-array.

4.2.2. Extensibility and Modular Deployment

The publish–subscribe communication model inherently supports the *mount-once, move-often* retrofitting strategy proposed in Section 1. The software architecture scales naturally: integrating a new sensor requires only an additional publisher node, while introducing a new processing algorithm requires only a corresponding subscriber. Furthermore, this modularity extends to external integration. Connection to host vessel machinery (e.g., actuators or engine status) can be realized via a gateway node that bridges vessel data streams to the common communication network. Similarly, additional sensors such as RADAR, (gyro)compass and wind anemometers, although not included in this sensor suite, can be integrated through dedicated publisher nodes, as they are commonly found on surface vessels. Finally, the location transparency of the underlying messaging system enables distributed deployment across the onboard network: computationally intensive perception modules can execute on the Sensor Box's IPC, while lightweight monitoring interfaces or vessel gateways can run on separate devices connected to the same network.

5. Reference Integration and Datasets

To validate the utility of *Sensor Box* as a vessel-agnostic reference infrastructure for autonomous functions, the system was deployed on the research vessel *Maverick* for field trials. This section (i) describes the hardware and software integration efforts required on the host vessel side (Section 5.1), and (ii) summarizes the specifications of the multimodal datasets collected (Section 5.2).

5.1. Reference Integration: Deployment on *Maverick*

The integration followed the modular principles outlined in Section 4. The fundamental requirement for the host vessel's side is twofold:

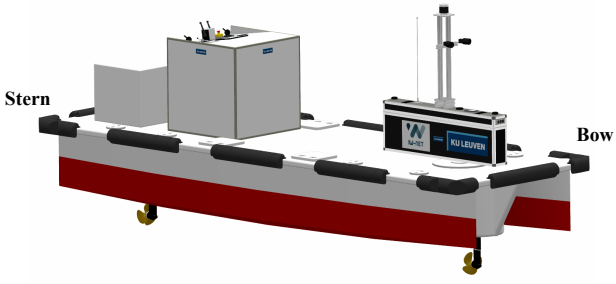

Figure 7: Joint Set-Up of *Maverick* Test Vessel and *Sensor Box*.

(i) **Hardware link:** provision of a suitable mounting location for *Sensor Box* and a network gateway that is reachable via an Ethernet cable.

(ii) **Software node:** standardization of the ship data stream and deployment of a bridge node that connects the vessel data stream to the messaging server running on *Sensor Box*.

5.1.1. Physical and Electrical Integration

For the physical deployment on research vessel *Maverick*, *Sensor Box* was secured along the centerline of the foredeck, as illustrated in Fig. 7. This configuration leverages the open deck of the host vessel and prioritizes perception performance by ensuring an unobstructed FOV of the fairway ahead.

For the broader European inland fleet, mounting locations must balance system performance with operational constraints. Two primary options are particularly relevant, each with distinct trade-offs:

(i) **Foredeck placement:** similar to the *Maverick* setup, foredeck mounting minimizes the near-field blind spot and is well suited for detecting small surface obstacles (e.g. buoys, debris). However, in commercial cargo operations this location exposes the hardware to potential collision damage and may interfere with necessary deck operations such as mooring and cargo handling.

(ii) **Wheelhouse placement:** positioning the unit on the roof of the wheelhouse (typically near the stern) offers a higher vantage point and reduces interference with deck operations. On long vessels, however, the large distance to the bow degrades the system's ability to detect obstacles directly ahead, and further elevating the sensors to compensate is often constrained by strict air-draft limits for bridge passage.

As for the electrical integration, *Maverick* features a mixed electrical topology as shown in Fig. 8, organized into distinct subsystems, using a combination of CAN-based protocols, analog, and digital signals. Importantly, *Sensor Box* does not interface with these subsystems individually. Instead, a PLC acts as a central aggregator, bridging the diverse legacy interfaces onto a common Ethernet network. *Sensor Box* connects to this architecture via a single Ethernet link to the onboard switch, providing a low-intrusion integration pattern that isolates the autonomy hardware from the vessel's wiring and high-power domains.

While *Maverick* represents a complex, research-oriented host vessel, the Ethernet-aggregated backbone is equally adaptable to industrial-oriented standard legacy architectures, such as those based on *NMEA 0183*, *NMEA 2000* or *SAE J1939* as discussed in Section 4.1.

5.1.2. Software Integration

The software integration follows the publish–subscribe communication model described in Section 4.2. To bridge between the messaging server and *Maverick*'s specific PLC registers, a dedicated software wrapper was deployed to bidirectionally translate messages between them following the Modbus-TCP Modbus Organization Inc. (2006) protocol. The data stream on *Maverick*'s side is referred to as the *PLC Stream*. This translation is governed by documented register maps that define the specific memory addresses to poll or write for each variable. Two topics were defined under *PLC Stream*:

(i) `plc.reader`: Overall vessel status, including feedback signals of thruster states, battery states, and readings of water-level sensors.

(ii) `plc.writer`: Control commands, including setpoint for the thrusters and auxiliary commands to toggle the bilge pumps.

This architecture leverages the software portability of the system. Autonomy algorithms interact with the standardized *PLC Stream*, remaining agnostic to the underlying Modbus-TCP implementation. Migrating *Sensor Box* to other vessels requires a similar integration effort: a new gateway node translates between the vessel's native protocol and the messaging server with vessel-specific standardization of data streams.

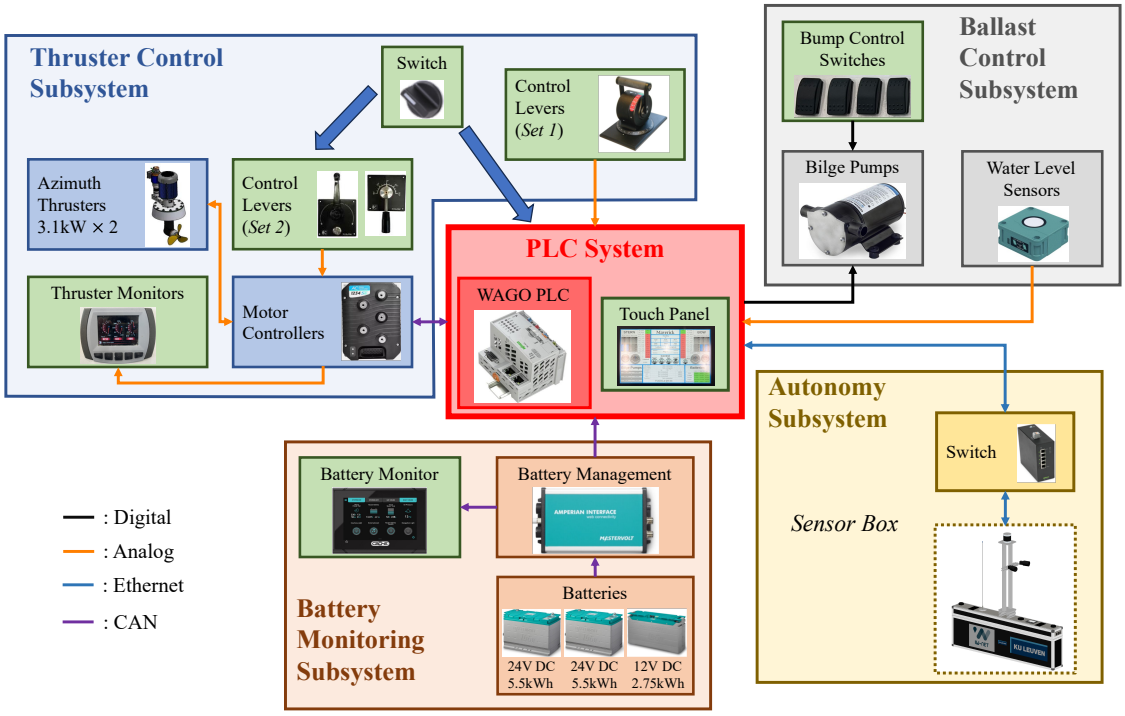

Figure 8: Electrical Integration Diagram of *Maverick*.

5.2. *Leuven Vaart Dataset*

We provide the *Leuven Vaart Dataset* to the research community. Collected using *Maverick*, this dataset comprises a synchronized multimodal data sequence covering a 1.3 km trajectory on *Kanaal Leuven-Dijle*. The recorded environment comprises a heterogeneous landscape of natural vegetated banks and concrete quay walls. The sequence also presents challenging perception scenarios, including fixed overhead bridge structures, a movable bascule bridge, variable lighting conditions, and dynamic surface objects such as waterfowl. The dataset includes LiDAR point clouds, stereo camera images, and GNSS/INS navigation data. However, AIS data is not included due to the absence of nearby AIS-equipped traffic during the recorded session. Representative samples of the synchronized sensor streams at three different locations are visualized in Fig. 9.

The dataset is organized into a hierarchical directory structure based on sensor modality, as illustrated in Fig. 10. Besides the `readme.md` file that summarizes the metadata of the dataset, the root directory contains four primary subfolders: `calibration`, `gnss_ins`, `lidar`, and `cameras`. The data files within these folders are detailed as follows:

(i) `Calibration`: This directory includes the system calibration parameters. `intrinsics.json` details the internal sensor models, including the camera projection matrices and distortion coefficients, as well as the IMU noise densities and bias random walk coefficients. `extrinsics.json` provides the rigid-body transformations mapping each sensor frame to the central body frame, along with their calibration uncertainties.

(ii) `gnss_ins`: This directory contains navigation data, including raw IMU and GNSS measurements, the fused GNSS/INS solution and the parsed NMEA strings. All streams are serialized as structured JSON files. Detailed descriptions of the individual data fields are provided in the accompanying `readme.md` located within this directory.

(iii) `lidar`: This directory stores the 3D point cloud data in the PCD format, as defined in Rusu and Cousins (2011). Each file represents a single LiDAR scan that contains point-wise attributes such as spatial coordinates (x, y, z), reflectance intensity, ring index, and a precise timestamp for motion de-skewing. Filenames follow the format `frame_points_<frame_id>_<timestamp>.pcd`, where the timestamp denotes the capture time in Unix epoch format.

(iv) `cameras`: This directory contains the visual data, organized into two subdirectories: `camera_1` and `camera_2`.

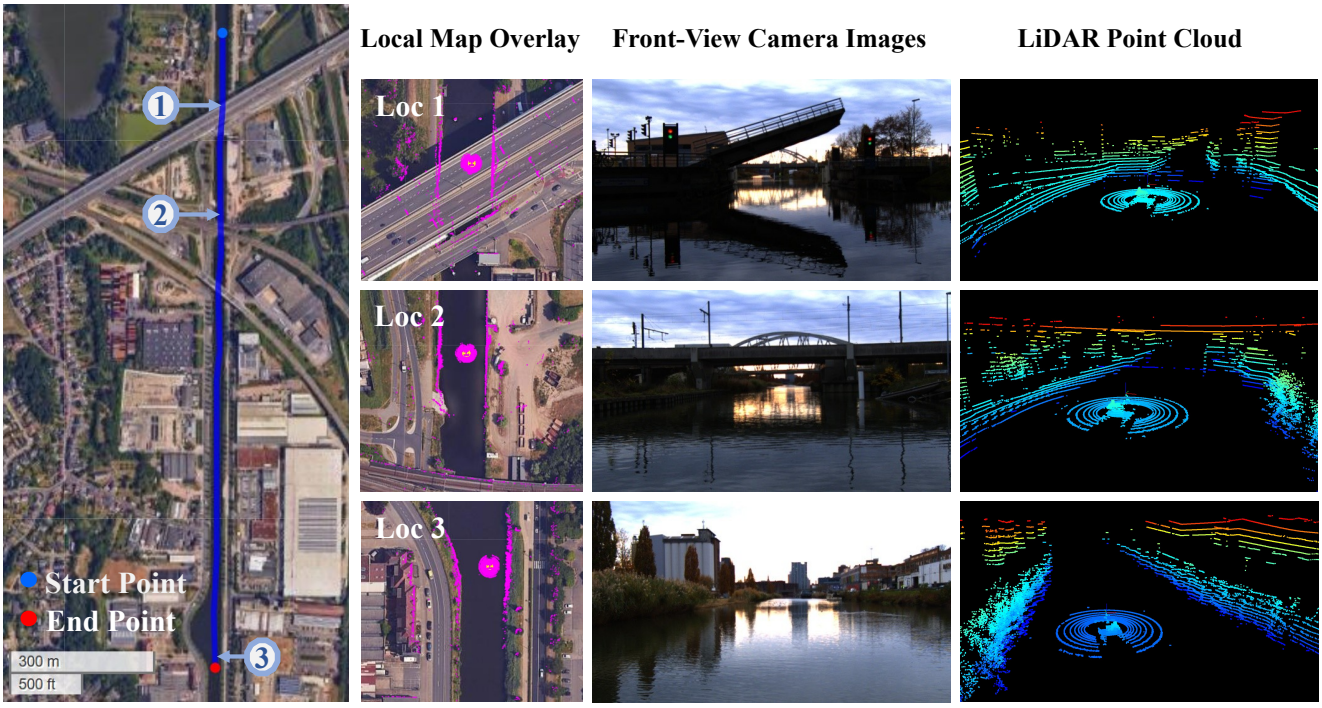

Figure 9: Visual summary of the *Leuven Vaart Dataset*. Left: The global vessel trajectory projected onto Google Maps, with three reference locations marked (1–3). Right: A matrix of synchronized sensor data snapshots corresponding to these locations. The columns display the 2D point cloud overlaid onto the local map, front-view camera images, and 3D LiDAR point clouds.

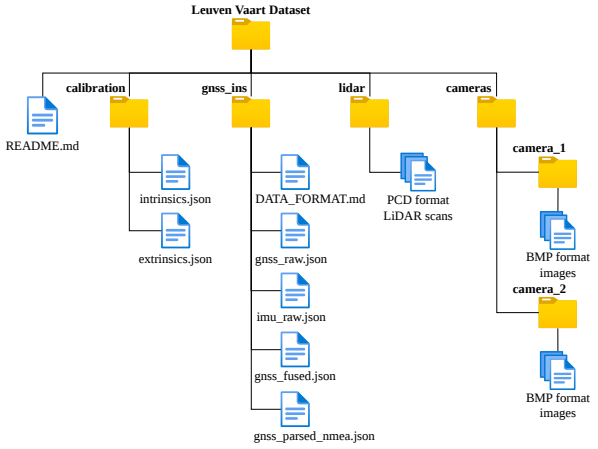

Figure 10: Hierarchical organization of the *Leuven Vaart Dataset*.

Images are stored as uncompressed Bitmap files containing raw BayerRG8 sensor data. Filenames encode both the trigger generation and host reception times to characterize latency, following the format `images_GGA_<start_ts>_End_<end_ts>.bmp`, where the timestamps are in Unix epoch format.

6. Conclusion

This paper addressed a key technical bottleneck in advancing autonomy development on European inland waterways: the lack of standardized, transferable onboard sensing and computing infrastructure for the heterogeneous and ageing inland fleet. Rather than proposing a new-build vessel, this work focused on enabling systematic experimentation through a modular, retrofitting-oriented, vessel-agnostic sensor suite, *Sensor Box*.

Sensor Box consolidates hardware components, including perception sensors, navigation instruments and communication devices, with onboard computation and power resources into a portable, self-contained unit that can be deployed across diverse vessels with minimal integration effort. Through its layered hardware design, system-level calibration and synchronization, and Ethernet-backboned NATS publish–subscribe communication architecture, the system enables real-time data acquisition and distribution, multi-sensor data fusion and processing within a unified spatial and temporal reference. The practical applicability of the platform was demonstrated through its deployment on the test vessel *Maverick* and the release of the openly accessible *Leuven Vaart Dataset*.

Although developed for inland waterway research, the underlying modular, standalone, and platform-agnostic design philosophy, is broadly transferable to other autonomous vehicle domains where retrofitting, standardized data acquisition, and portability are required.

Future work will focus on extending *Sensor Box* deployment to additional vessels and operational scenarios, further validating its vessel-agnostic concept, and on further extending the publicly available dataset. By providing a standardized research platform and multimodal data foundation, this work contributes toward a shared experimental ecosystem supporting reproducible studies of autonomous navigation in inland waterways and beyond.

Acknowledgement

The authors gratefully acknowledge colleagues who contributed substantially to the development of Sensor Box, including Jiangtao Shuai, Thibaut Schamp, and Pascal Carreweyn.

CRediT authorship contribution statement

Yan Yun, Zhang: Conceptualization, Visualization, Data curation, Writing - original draft, Writing - review & editing. **Zhongbi Luo:** Data curation, Visualization, Writing - original draft. **Jef Billet:** Conceptualization, Writing - original draft. **Senne Van Baelen:** Software. **Jan Swevers:** Supervision, Writing - review & editing. **Herman Bruyninckx:** Supervision, Writing - review & editing. **Peter Slaets:** Supervision, Resources, Funding acquisition, Writing - review & editing.

Declaration of generative AI and AI-assisted technologies in the manuscript preparation process

During the preparation of this work, Google Gemini 3.0 was used by the second author to debug and refine the plotting scripts for Fig. 4. After using this tool, the author reviewed and edited the content as needed and takes full responsibility for the content of the published article.

References

Alfheim, H.L., Muggerud, K., Breivik, M., Brekke, E.F., Eide, E., Engelhardtsen, Ø., 2018. Development of a dynamic positioning system for the ReVolt model ship. IFAC-PapersOnLine 51, 116–121. doi:10.1016/j.ifacol.2018.09.479.

Allan, D.W., 1966. Statistics of atomic frequency standards. Proceedings of the IEEE 54, 221–230. doi:10.1109/PROC.1966.4634.

Allis, M.J., Peirson, W.L., Banner, M.L., 2011. Application of LiDAR as a measurement tool for waves, in: Proceedings of the 21st International Ocean and Polar Engineering Conference (ISOPE), The International Society of Offshore and Polar Engineers. doi:10.1109/ISOPE.2011.6102218.

Analog Devices, . ADIS16505 datasheet and product information. https://www.analog.com/en/products/adis16505.html, accessed 2025-07-30.

Baerveldt, M., Shuai, J., Brekke, E.F., 2024. Improved fusion of ais data for multiple extended object tracking, in: Proceedings of the 27th International Conference on Information Fusion (FUSION), IEEE. pp. 1–8.

Baumer, . Industrial cameras / CX series VCXG.2-51C.I: Cameras for demanding image processing tasks. https://www.baumer.com/be/en/product-overview/industrial-cameras-image-processing/industrial-cameras/cx-series/vcx-i-cameras/cameras-for-demanding-image-processing-tasks/vcxg-i/vcxg-2-51c-i/p/46438, accessed 2025-07-30.

Brekke, E.F., Eide, E., Eriksen, B.O.H., Wilthil, E.F., Breivik, M., Skjellaug, E., Helgesen, Ø.K., Lekkas, A.M., Martinsen, A.B., Thyri, E.H., Torben, T., Veitch, E., Alsos, O.A., Johansen, T.A., 2022. milliAmpere: an autonomous ferry prototype. Journal of Physics: Conference Series 2311, 012029. doi:10.1088/1742-6596/2311/1/012029.

Buchanan, R., 2021. Allan Variance ROS. Oxford Robotics Institute, DRS Lab. https://github.com/ori-drs/allan_variance_ros. Version 1.2.

Chen, Z., Qi, Y., Feng, D., Zhuang, X., Chen, H., Hu, X., Wu, J., Peng, K., Lu, P., 2025. Heterogeneous LiDAR dataset for benchmarking robust localization in diverse degenerate scenarios. The International Journal of Robotics Research 45, 6–22. doi:10.1177/02783649251344967.

Curnow, R., Lichvar, M., 2025. Chrony: A versatile implementation of the Network Time Protocol. https://chrony-project.org. Version 4.8.

Eide, E., Breivik, M., Brekke, E.F., Eriksen, B.O.H., Wilthil, E., Helgesen, Ø.K., Thyri, E.H., Veitch, E., Alsos, O.A., Johansen, T.A., 2025. The autonomous urban passenger ferry milliAmpere2: Design and testing. Journal of Offshore Mechanics and Arctic Engineering 147, 031409. doi:10.1115/1.4067370.

Esposito, F., 2024. Inland Navigation in Europe: Market Observation. Annual Report. European Inland Waterway Transport Platform. https://www.inlandwaterwaytransport.eu/wp-content/uploads/Annual-Report-2024-_-European-IWT-Platfrom_last_.pdf, accessed 2026-02-11.

Eurostat, 2026. Length of navigable inland waterways by waterway type. doi:10.2908/iww_if_infrastr. https://ec.europa.eu/eurostat/databrowser/view/iww_if_infrastr/default/table?lang=en&category=iww.iww_if, accessed 2026-02-11.

Furgale, P., Rehder, J., Siegwart, R., 2013. Unified temporal and spatial calibration for multi-sensor systems, in: Proceedings of the 2013 IEEE/RSJ International Conference on Intelligent Robots and Systems (IROS), Tokyo, Japan. pp. 1280–1286. doi:10.1109/IROS.2013.6696514.

Gbako, S., Paraskevadakis, D., Ren, J., Wang, J., Radmilovic, Z., 2025. A systematic literature review of technological developments and challenges for inland waterways freight transport in intermodal supply chain management. Benchmarking: An International Journal 32, 398–431. doi:10.1108/BIJ-03-2023-0164.

Helgesen, Ø.K., Vasstein, K., Brekke, E.F., Stahl, A., 2022. Heterogeneous multi-sensor tracking for an autonomous surface vehicle in a littoral

environment. Ocean Engineering 252, 111168. doi:10.1016/j.oceaneng.2022.111168.

Homburger, H., Wirtensohn, S., Diehl, M., Reuter, J., 2024. Energy-optimal planning and shrinking horizon mpc for vessel docking in river current fields, in: Proceedings of the 2024 European Control Conference (ECC), IEEE, Stockholm, Sweden. pp. 1125–1130. doi:10.23919/ECC64448.2024.10591279.

Homburger, H., Wirtensohn, S., Hoher, P., Baur, T., Griesser, D., Diehl, M., Reuter, J., 2025. Solgenia—A test vessel toward energy-efficient autonomous water taxi applications. Ocean Engineering 328, 121011. doi:10.1016/j.oceaneng.2025.121011.

International Electrotechnical Commission, 2024. Maritime navigation and radiocommunication equipment and systems — Digital interfaces — Part 450: Multiple talkers and multiple listeners — Ethernet interconnection. https://webstore.iec.ch/en/publication/72731. Version 3.0.

Li, S., Liu, J., Negenborn, R.R., Wu, Q., 2020. Automatic docking for underactuated ships based on multi-objective nonlinear model predictive control. IEEE Access 8, 70044–70057. doi:10.1109/ACCESS.2020.2984812.

Luo, Z., Van Baelen, S., Slaets, P., Bruyninckx, H., 2024. Enhancing inland waterway transport through LiDAR-based updates to electronic navigational charts, in: Proceedings of OCEANS 2024 - Halifax, IEEE, Halifax, Canada. pp. 01–08. doi:10.1109/OCEANS55160.2024.10754408.

MathWorks, 2025. Camera Calibration Toolbox. The MathWorks, Inc.. Natick, Massachusetts, USA. https://www.mathworks.com/help/vision/camera-calibration.html. Version R2025b.

Modbus Organization Inc., 2006. Modbus messaging on TCP/IP implementation guide. https://www.modbus.org/docs/Modbus_Messaging_Implementation_Guide_V1_0b.pdf. Version 1.0b.

National Marine Electronics Association, 2022. NMEA 2000 interface standard for marine electronic equipment based on CAN communications. https://www.nmea.org/nmea-2000.html. Version 3.000.

National Marine Electronics Association, 2023. NMEA 0183 interface standard for marine electronic equipment based on serial data bus. https://www.nmea.org/nmea-0183.html. Version 4.30.

National Marine Electronics Association, 2024. NMEA OneNet standard for IP networking of marine electronic devices. https://www.nmea.org/nmea-onenet.html. Version 1.002.

Némethy, S.A., Ternell, A., Bornmalm, L., Lagerqvist, B., Szemethy, L., 2022. Environmental viability analysis of connected European inland–marine waterways and their services in view of climate change. Atmosphere 13, 951. doi:10.3390/atmos13060951.

Peeters, G., Kotzé, M., Afzal, M.R., Catoor, T., Van Baelen, S., Geenen, P., Vanierschot, M., Boonen, R., Slaets, P., 2020. An unmanned inland cargo vessel: Design, build, and experiments. Ocean Engineering 201, 107056. doi:10.1016/j.oceaneng.2020.107056.

RoboSense, . Helios series: A new generation of customized LiDAR platform, including 32-beam and 16-beam LiDAR. https://www.robosense.ai/en/IncrementalComponents/Helios, accessed 2025-07-30.

Rusu, R.B., Cousins, S., 2011. 3D is here: Point Cloud Library (PCL), in: Proceedings of the 2011 IEEE International Conference on Robotics and Automation (ICRA), Shanghai, China. pp. 1–4. doi:10.1109/ICRA.2011.5980567.

SAE International, 2023. SAE standard J1939 — Serial control and communications heavy-duty vehicle network. https://www.sae.org/standards/j1939_202306-serial-control-communications-heavy-duty-vehicle-network-top-level-document. Version 202306.

Septentrio, . AsteRx-i3 D Pro + GNSS/INS Receiver. https://www.septentrio.com/en/products/gnss-ins-receivers/gnss-ins-boards/asterx-i3-d-pro-plus, accessed 2025-07-30.

Septentrio, 2024. RxTools: GNSS receiver control and analysis software. https://www.septentrio.com/en/products/gps-gnss-receiver-software/rxtools. Version 24.0.0.

Synadia Communications Inc., 2025. NATS server: High-performance cloud native messaging system. https://nats.io/. Version 2.11.

Wang, W., Fernández-Gutiérrez, D., Doornbusch, R., Jordan, J., Shan, T., Leoni, P., Hagemann, N., Schiphorst, J.K., Duarte, F., Ratti, C., Rus, D., 2023. Roboat III: An autonomous surface vessel for urban transportation. Journal of Field Robotics 40, 1996–2009. doi:10.1002/rob.22237.

Wang, W., Shan, T., Leoni, P., Fernández-Gutiérrez, D., Meyers, D., Ratti, C., Rus, D., 2020. Roboat II: A novel autonomous surface vessel for urban environments, in: Proceedings of the 2020 IEEE/RSJ International Conference on Intelligent Robots and Systems (IROS), Las Vegas, NV, USA. pp. 1740–1747. doi:10.1109/IROS45743.2020.9340712.

Zhang, Y.Y., Billet, J., Slaets, P., 2024. Experimental identification of decoupled ship dynamic models for an autonomous catamaran urban cargo vessel. IFAC-PapersOnLine 58, 229–234.

Zhang, Y.Y., Shuai, J., Billet, J., Slaets, P., 2023. Design and build of an autonomous catamaran urban cargo vessel. Journal of Physics: Conference Series 2618, 012002. doi:10.1088/1742-6596/2618/1/012002.

Zheng, C., Zhang, F., 2025. FAST-Calib: LiDAR-Camera extrinsic calibration in one second. arXiv preprint, arXiv:2507.17210. Available at: https://arxiv.org/abs/2507.17210.